

**Imaging the dynamics of an individual hydrogen atom intercalated between two graphene sheets**Wen-Xiao Wang,<sup>1</sup> Yi-Wen Wei,<sup>2</sup> Si-Yu Li,<sup>1</sup> Xinqi Li,<sup>3</sup> Xiaosong Wu,<sup>3</sup> Ji Feng,<sup>2,\*</sup> and Lin He<sup>1,\*</sup><sup>1</sup>*Center for Advanced Quantum Studies, Department of Physics, Beijing Normal University, Beijing, 100875, People's Republic of China*<sup>2</sup>*International Center for Quantum Materials, School of Physics, Peking University, Beijing 100871, People's Republic of China*<sup>3</sup>*State Key Laboratory for Artificial Microstructure and Mesoscopic Physics, Peking University, Beijing 100871, China and Collaborative Innovation Centre of Quantum Matter, Beijing 100871, China*

(Received 16 October 2017; revised manuscript received 24 December 2017; published 6 February 2018)

The interlayer gallery between two adjacent sheets of van der Waals materials is expected to modify properties of atoms and molecules confined at the atomic interfaces. Here, we directly image individual hydrogen atom intercalated between two graphene sheets and investigate its dynamics by scanning tunnelling microscopy (STM). The intercalated hydrogen atom is found to be remarkably different from atomic hydrogen chemisorbed on the external surface of graphene. Our STM measurements, complemented by first-principles calculations, show that the hydrogen atom intercalated between two graphene sheets has dramatically reduced potential barriers for elementary migration steps. Especially, the confined atomic hydrogen dissociation energy from one of the graphene sheet is reduced to 0.34 eV, which is only about a third of a hydrogen atom chemisorbed on the external surface of graphene. This offers a unique platform for direct imaging of the atomic dynamics of confined atoms. Our results suggest that the atomic interfaces of van der Waals materials provide a confined environment to tune the dynamics process of confined atoms or molecules.

DOI: [10.1103/PhysRevB.97.085407](https://doi.org/10.1103/PhysRevB.97.085407)

Two-dimensional (2D) materials, such as graphene, expose all the atoms to the surfaces, therefore, adsorbed atoms or molecules can dramatically change their atomic and electronic structures [1–7]. For example, hydrogen atoms adsorbed on graphene can generate energy gaps [1,2] and even induce magnetic moments [4–6] in graphene. Although the strong influence of adsorbates on graphene has attracted tremendous interest, the effects of graphene on the adsorbed atoms or molecules are much less explored. Very recently, several groups began to study effect of interlayer gallery between two graphene sheets on entrapped atoms and molecules, and demonstrated that the confined space can modify their structures and properties [8–10]. However, probing the dynamics and chemical reaction of atoms intercalated in van der Waals materials proves extremely challenging. Here, we directly image an individual hydrogen atom intercalated between two graphene sheets and study its dynamics by using scanning tunnelling microscopy (STM). Our result demonstrates that the hydrogen atom confined at the atomic interface behaves remarkably different from that chemisorbed on the surface of graphene. For the former case, the hydrogen atom between two graphene sheets is found to be extraordinarily mobile at 80 K, which can be further enhanced by the STM tip, to allow for observation of migratory dynamics, whereas the chemisorbed hydrogen on the surface of graphene is localized at such a low temperature. Our first-principles calculations indicate that potential barriers for hydrogen dynamics, especially the barriers for desorption, are much reduced when the hydrogen atom is confined between two graphene sheets.

The scanning tunneling microscopy (STM) system is an ultrahigh vacuum single-probe scanning probe microscope (USM-1500) from UNISOKU. All STM measurements were performed at liquid-nitrogen temperature and the images were taken in a constant-current scanning mode. The STM tips were obtained by chemical etching from a wire of Pt(80%) Ir(20%) alloys. Lateral dimensions observed in the STM images were calibrated using a standard graphene lattice as well as a Si (111)-(7 × 7) lattice.

The spin-polarized density functional theory (DFT) calculations were performed with the Vienna *ab initio* simulation package (VASP) [11,12], using the projector augmented wave (PAW) potentials [13,14]. The electron-electron exchange correlation was approximated by the generalized gradient functional of Perdew-Burke-Ernzerhof (PBE) [15]. We used a vacuum space of 1.5 nm along the *z* direction. A cutoff energy of 400 eV was used together with a Gamma centered  $8 \times 8 \times 1k$ -point grid [16] for a (4 × 4) supercell containing 64 carbon atoms of bilayer graphene. The van der Waals interactions were described via the DFT-D2 method of Grimme [17]. To compute the barriers, the climbing-image nudged elastic band (CI-NEB) method is used to find the minimum energy paths, which starts from the interpolated configurations between initial and final states with reaction coordinates to label system configurations along the reaction pathway [18,19]. After relaxation and optimization, the separations between the graphene layers are about 3.3 Å. In the stable structures, C-H bond lengths are 1.12 Å for layer1(A)-layer2(B) and layer1(A)-layer1(B); 1.13 Å for layer1(B)-layer2(A), respectively. STM images were simulated using the Tersoff-Hamann formalism with a (8 × 8) supercell (256 carbon atoms) of bilayer graphene.

In this work, the bilayer graphene was grown on the SiC by thermal decomposition with the hydrogen assisted growth

\*To whom correspondence may be addressed: jfeng11@pku.edu.cn; helin@bnu.edu.cn

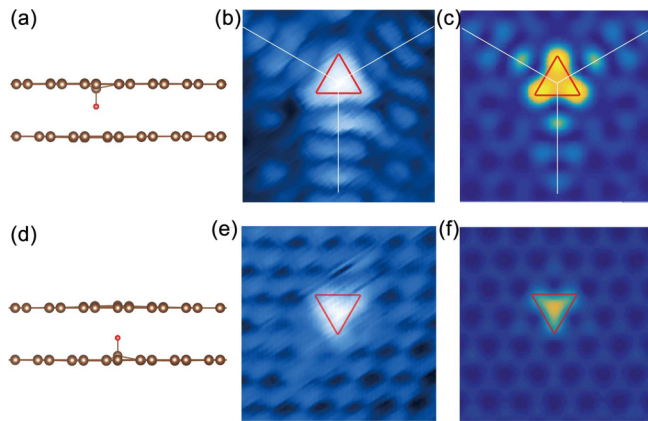


FIG. 1. The structure of H confined between graphene layers. [(a) and (d)] The side view for ball-and-stick model of bilayer graphene showing the position of the H atom adsorbing. The red ball denotes the hydrogen atom. [(b) and (e)] Typical atomic STM images of hydrogen atom chemisorbed on epitaxial graphene on SiC(000 $\bar{1}$ ), corresponding to schematic diagrams shown in (a) and (d), respectively. Sample bias and set points are (0.4 V, 300 pA) and (0.07 V, 300 pA), respectively. The honeycomb structures of graphene are overlaid onto the STM images. [(c) and (f)] The simulated STM images at comparable imaging conditions show similar features to that in (b) and (e), respectively. Image size is 1.48 nm  $\times$  1.48 nm.

method. The hydrogen, as a carbon etchant, not only suppresses the growth of multilayer graphene, but also suppresses the defect formation and nucleation of graphene [20]. By controlling the hydrogen concentration and growth time, we successfully synthesized the bilayer graphene with smooth surface morphology. The Raman spectroscopy spectrum of the sample (Fig. S1 [21]) shows the absence of the D peak and almost the same intensities of the G and 2D peaks. Such a result demonstrated explicitly that the synthesized sample is high quality bilayer graphene [22,23]. We chose to study hydrogen atoms confined between two graphene sheets based on following reasons. (i) The hydrogen atoms exist naturally in the sample synthesized by our method (they are generated in the dissociation process of both CH<sub>4</sub> and H<sub>2</sub> at temperature above 1500 °C). (ii) It is convenient to identify the chemisorbed hydrogen atoms, the simplest adsorbate species, on graphene by using STM. (iii) The chemisorption and desorption of individual hydrogen atoms on graphene, to some extents, maybe the simplest chemical reaction confined between two graphene sheets, which can be treated as a model system to study the interfacial chemical reactions.

The hydrogen intercalation of graphene on SiC was extensively studied previously [24–26]. However, these studies mainly focus on graphene grown on the Si surface of SiC and the introduced hydrogen atoms bond with the Si atoms to release the buffer layer. Obviously, this quite differs from the studied structure in our work. Here, the graphene bilayer was grown on the C surface of SiC and, importantly, the hydrogen atoms intercalate between two graphene sheets instead of bonding with the Si atoms. There are multiple local potential energy minima for the hydrogen atom intercalated between two graphene sheets. It could be attached to either the first or the second layer, as illustrated in Figs. 1(a) and 1(d) (side views). The obtained STM images for the two cases are

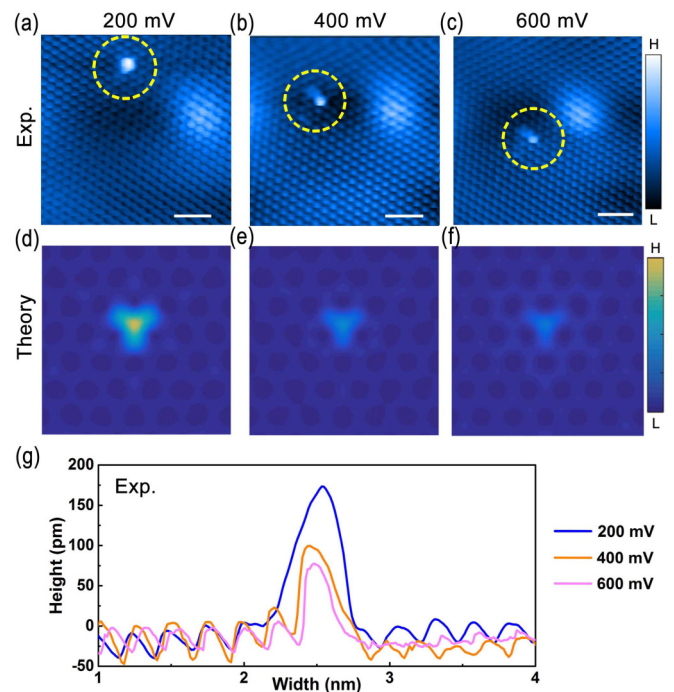


FIG. 2. The height of H intercalated between graphene bilayer. (a)–(c) Atomic STM images of hydrogen atom (highlighted by a yellow circle) chemisorbed on the second layer of graphene. The images are recorded at sample bias of 200, 400, and 600 mV, respectively. The larger and stable bright protrusion may arise from defects of the SiC substrate. (d)–(f) The corresponding simulated images at comparable imaging conditions to that of (a)–(c). They are adjusted into the same contrast for better comparison. (g) shows the profile lines across the hydrogen atom of panels (a)–(c). The scale bar for (a)–(c) is 1 nm. The image size for (d)–(f) is 1.48 nm  $\times$  1.48 nm.

quite different. In the former case, the high-resolution STM image [Fig. 1(b)] exhibits threefold symmetry because the  $p_z$  orbitals of the three nearest neighboring carbon atoms contribute the local states. A  $\sqrt{3} \times \sqrt{3}R30^\circ$  (R3) interference pattern attributed to the elastic scattering process between  $K$  and  $K'$  valley is also observed around the hydrogen atom [27,28]. These experimental features are well reproduced in our simulated STM image [Fig. 1(c)]. The major features of our experimental result, such as a bright triangle center and the interference pattern around the chemisorbed H, are similar to those reported for H chemisorbed on the external surface of graphene in previous studies [4,6]. In the latter case [Fig. 1(d)], the intercalated hydrogen atom in the STM image becomes an atomic-sized bright dot, as shown in Fig. 1(e). Such an experimental feature and the bias dependent STM images, as shown in Fig. 2, are also reproduced quite well by the corresponding simulated images shown in Figs. 1(f) and 2(d)–2(f). Therefore isolated hydrogen atom confined between bilayer graphene exhibits different features when chemisorbed on the first and the second layer. In a previous study, the hydrogen adsorbing on graphene could induce a localized state in the system [4–6]. Here we also observe the same feature for the intercalated hydrogen, as shown in Fig. S2 [21]. The STS spectrum shows a resonance peak at the charge neutrality point near the chemisorbed hydrogen. Such a result

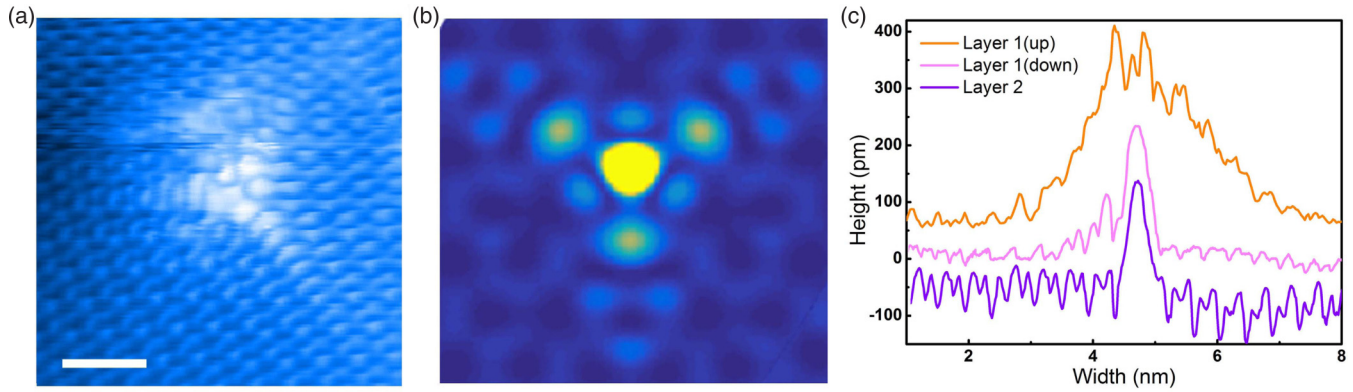


FIG. 3. (a) The typical STM image of the H atom adsorbed on the outer surface of the topmost graphene layer. Sample bias and setpoint are (50 mV, 200 pA). Scale bar is 1 nm. (b) The simulated STM image at comparable imaging conditions to (a). (c) The shifted profile lines across the H corresponding to the H atom adsorbed on a different layer: outer surface of the layer1 (red line); inner surface of the layer1 (pink line); and layer 2 (purple line). It is clear that the H atom adsorbed on the outer surface of layer 1 graphene is much higher and wider in the STM image.

is also reproduced well in our theoretical calculation (Fig. S2 [21]).

We can exclude atomic defects, substitutional atoms, and other types of intercalation species as the origin of the experimental features in Fig. 1. A single carbon vacancy can generate similar features in graphene except that the local symmetry is broken due to the Jahn-Teller distortion [29] (Fig. S3 [21]). This slight difference could help us to distinguish them in the STM measurements. The substitutional atoms, for example, the N substitution [30,31], are very stable and localized, which is distinct from our experimental observation and allow us to completely rule them out. The other possible intercalation species, such as the O, Si, and Ne atoms, exhibit quite different features, like a bright “blister” and without apparent scattering pattern [32–34], in the STM measurements comparing to that of H chemisorbed on graphene. We can also rule out the hydrogen atom chemisorbed on the external surface of the first layer as the origin of the observed features in Fig. 1 based on the following three experimental results. First, the hydrogen atom on the surface of graphene would have a higher height profile,  $>250$  pm, than the topographically small features observed,  $<200$  pm (see Figs. 2, 3, and S2 for details). Second, the hydrogen atom on the external surface of graphene would possibly get swept away by the STM tip during the measurements when we used a large bias, such as 2–5V. However, this does not happen during our STM measurements for more than 30 hours. Third, in our experiment, we frequently observed transition of the hydrogen atom between chemisorbed on the first layer and the second layer, i.e., the recorded STM images of the adatom changes between that of Fig. 1(b) and that of Fig. 1(e).

The above results demonstrated explicitly that the hydrogen atom intercalated between the two graphene sheets is the origin of the observed features in our STM measurements. Then a question arises as to how the hydrogen atoms intercalate into the two graphene sheets. Previously, it was proposed that external atoms could intercalate graphene through edges of graphene islands or pre-existing defects in graphene [35–37]. In our experiment, the studied graphene bilayer is continuous, which helps us to exclude the edges of graphene island as the possible route for the intercalation. Although we do not

observe obvious defects in the studied region in our STM measurements (see Fig. S2 [21]), it is well-known that defects are almost inevitable in the synthesized graphene samples. The hydrogen atoms maybe intercalate into the two graphene sheets through the defects not in the studied region and diffuse into the studied area.

Unlike single carbon vacancies, which are difficult to generate in graphene (the formation energy is as high as about 7.4 eV) [29,38,39], the hydrogen atoms are very easy to chemisorb on graphene (the surface adsorption barrier on graphene is only about 0.2 eV) [1,2,5,6,40–42]. However, to break the C-H bond for chemisorbed hydrogen dissociation from graphene, one has to overcome a relatively higher potential barrier of about 1.1 eV [43–45]. Therefore the chemisorbed hydrogen atoms on the external surface of graphene are quite stable at low temperature. At 80 K (the temperature at which our experiments were performed), we find that they can be stable for more than 10 hours during the STM measurements (with small bias). This stabilization allows the patterning and characterization of the chemisorbed hydrogen atoms on external surface of graphene by using STM in previous studies [6,42].

For the hydrogen atom confined between two graphene sheets, however, our experiment indicates that it is quite easy to observe its desorption and migration even when we carried out STM measurements with small bias. Figure 4 shows a representative diffusion process of the H atom (highlighted by yellow circle) chemisorbed on the second graphene layer, in which the arrows roughly denote the moving directions. Obviously, the H atom changes its positions continuously during the STM measurement. For the structure shown in Fig. 4, there are two advantages to study the dynamics of the single hydrogen atom. First, there are two stable and slightly separated bright protrusions, as shown in Fig. 4(a), which may arise from defects of the substrate. This enables us to explicitly define the relative positions of the hydrogen atom. Second, there is not very high density of hydrogen atom (see Fig. S2 [21]) in the studied region  $\sim 50$  nm  $\times$  50 nm. We could focus on one individual atom and trace the dynamics of the hydrogen atom every time. In our STM measurements with low bias voltages, we observed the diffusion processes occasionally and

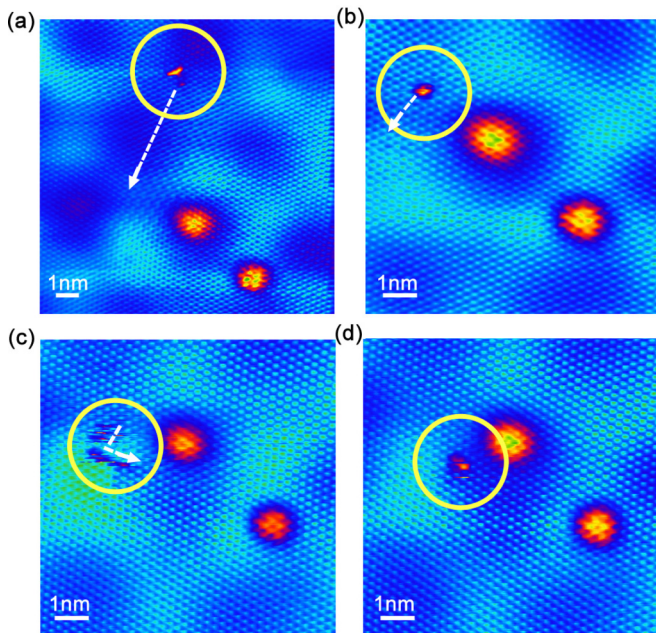


FIG. 4. The diffusion of the confined hydrogen atom. (a)–(d) Several representative STM images showing the diffusion process of the confined hydrogen atom (highlighted by yellow circle) at 80 K. Sample bias and set points for (a), (b), and (d) are (0.6 V, 300 pA); for C, they are (1 V, 300 pA).

randomly. However, by using a bias voltage or bias pulse larger than 1 V, we can stimulate the hydrogen atom locked between the two graphene sheets and observe its dynamics in a more controlled way (see Fig. 4 and supplementary movies [21]). By using this method, we can even capture the moving path of the H atom during scanning at bias of 1 V [see Fig. 4(c) and Fig. S4 [21]].

Besides the diffusion of the confined H atom, we also frequently observed transition of the hydrogen atom between chemisorbed on the first layer and the second layer in our experiment. Figure 5 shows several typical STM images recorded consecutively in our experiment. In Fig. 5(a), the hydrogen atom chemisorbed on the inner surface of the first layer. It chemisorbed on the second layer in Fig. 5(c). Interestingly, we observe the in-between state in Fig. 5(b), where the hydrogen atom desorbed from the first layer and then chemisorbed on the second layer. Such a process is also explicitly shown in Fig. 5(f) by the profile lines across the hydrogen atom. It is very interesting to note that all the R3 scatter patterns generated by the H atom chemisorbed on the first layer are in the same direction in our experiment [see Figs. 5(a) and 5(d) for examples]. Because of that the directions of R3 scatter patterns for H chemisorbed on two sublattices of graphene are different, as shown in Fig. S5 [21], we can conclude that the H prefers to adsorb one kind of sublattice of the first graphene sheet. Such a feature is quite different from that of hydrogen atom chemisorbed on the external surface of graphene, where

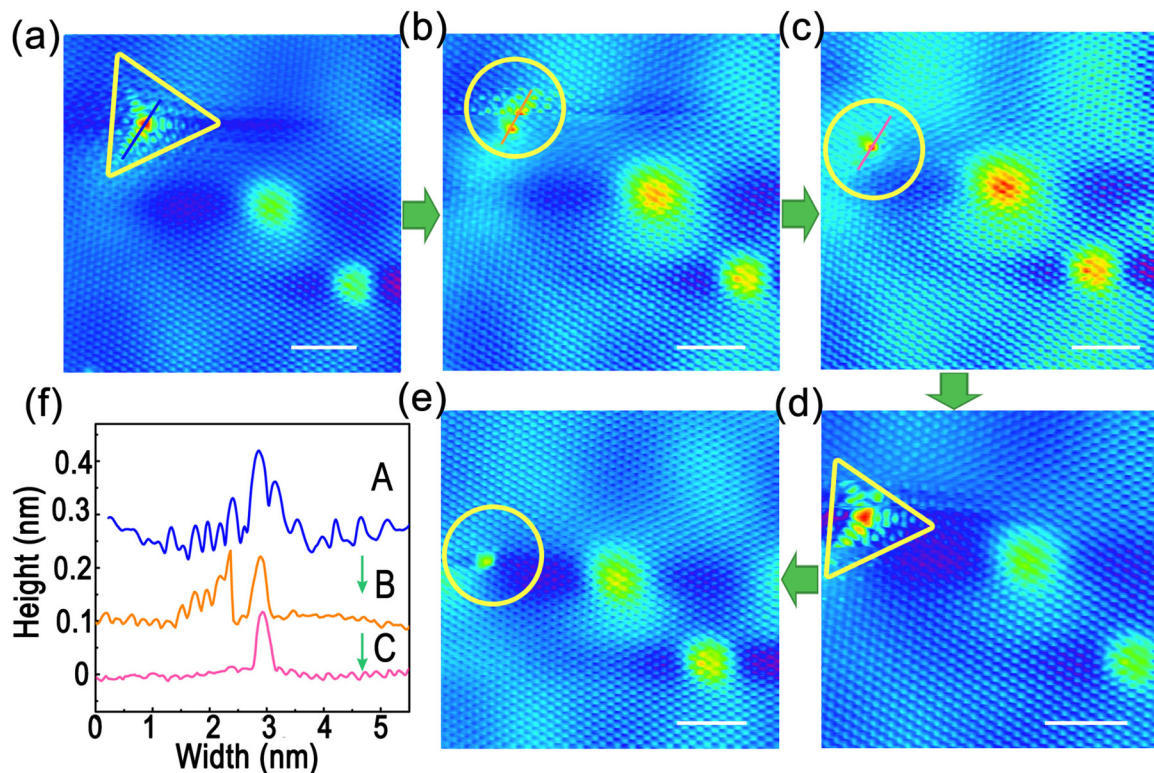


FIG. 5. The desorption and chemisorption processes of the confined H atom. (a) The hydrogen atom chemisorbed on the inner surface of the first layer. (b) The in-between state of the hydrogen atom, which changes from that chemisorbed on the inner surface of the first layer to that chemisorbed on the second layer. (c) The hydrogen atom chemisorbed on the second layer. [(d) and (e)] The hydrogen atom chemisorbed on the inner surface of the first layer and chemisorbed on the second layer, respectively. The sample bias and set point are (0.4 V, 300 pA) for (a)–(d), and (0.6 V, 300 pA) for (e). The scale bar is 2 nm. We use a triangle and a circle to denote a hydrogen atom chemisorbed on the inner surface of the first layer and one chemisorbed on the second layer, respectively. (f) Line profiles across the H atom taken from (a)–(c) to illustrate the topographic changes.

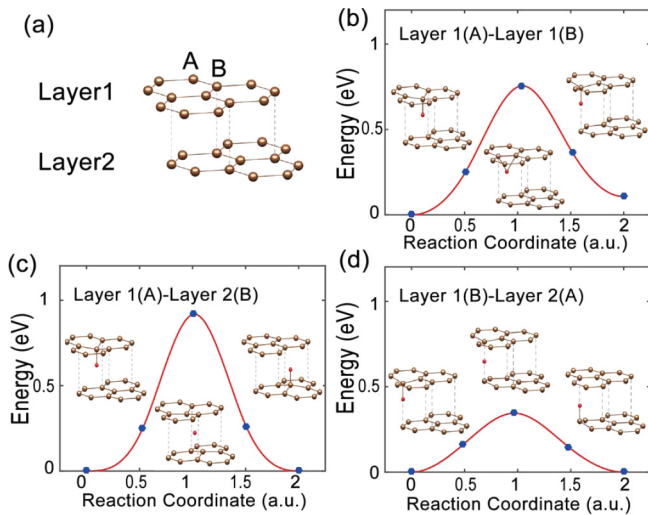


FIG. 6. Energy barriers of diffusion and desorption for the confined H atom. (a) Lattice structure of pristine bilayer graphene in Bernal stacking (side view). The up layer named layer 1, the down layer named layer 2. Two hexagonal sublattices are labeled as A and B. The red ball denotes H atom. (b) The computed barrier for migration of hydrogen atom from A site to B site on the top layer. (c) Hydrogen atom migration barrier from layer 1(A) sublattice to layer 2(B) site. During the calculation, one atom in each of two layers for in-plane direction is fixed to avoid the translation between the two layers. However, the atoms are still free in vertical direction, which allows the changing of graphene-graphene separation during the structural relaxation. (d) Hydrogen atom migration barrier from layer 1(B) site to layer 2(A) site.

the probabilities for the two sublattices should be equal. We will demonstrate subsequently that this feature is a direct experimental result of the H atom intercalated between two graphene sheets.

The above result clearly indicates that the potential barriers of diffusion and desorption are much reduced for the confined hydrogen atom. To validate this hypothesis, we calculated the diffusion and desorption processes of a hydrogen atom (a) chemisorbed on the external surface of graphene and (b) intercalated between two graphene sheets (Fig. 6). In the calculations, the two graphene sheets: layer 1 (up layer) and layer 2 (down layer) are assumed to be Bernal stacked as shown in Fig. 6(a) and effects of the substrate are ignored. From the calculation, we can see that the barrier of diffusion for a hydrogen atom chemisorbed on the external surface of graphene is about 1.02 eV (Fig. S6 [21]), whereas the barrier of diffusion for a confined hydrogen atom is only 0.75 eV, as shown in Fig. 6(b). Our calculation, as illustrated in Fig. 7, further indicates that an effective electric field on the sample may further reduce the barrier. In the experiment, both the STM tip and substrate could generate an effective electric field on the sample [46–48]. In our STM measurements, we observe the dynamics of the hydrogen atom more frequently by using a bias voltage larger than 1 V, which may partially arise from the lowering of the potential barrier induced by the effective electric field. Obviously, these barrier reductions could promote the diffusion of the hydrogen atom locked between the two graphene sheets.

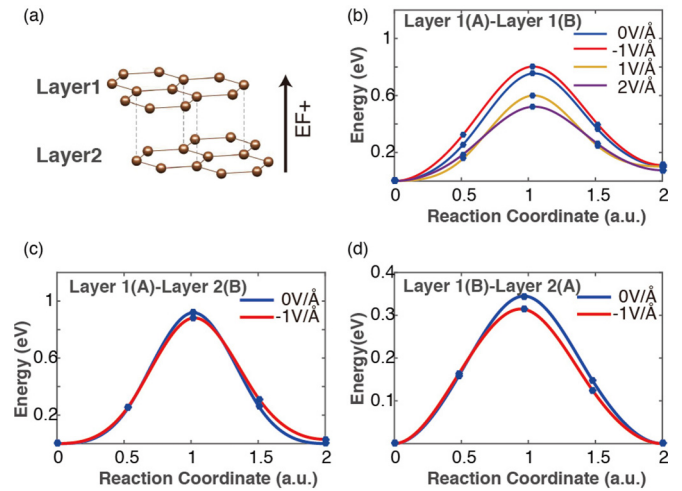


FIG. 7. The influence of the electric field on the transferred process of the H atom between bilayers of graphene. (a) Schematic diagram to illustrate the direction of the electric field. (b)–(d) The effect of the different electric field on the processes of layer1(A)-layer1(B), layer1(A)-layer2(B), and layer1(B)-layer2(A), respectively.

For a hydrogen atom chemisorbed on the external surface of graphene, the potential barrier of desorption is about 1.1 eV [43,44]. Our calculation indicates that the potential barrier is reduced if the hydrogen atom is locked between two graphene sheets. In the calculation, where the carbon atoms are allowed to relax, the interlayer separation is 3.3 Å, which is comparable to the previous study [49]. There are two possible and basic routes for the desorption process of the confined hydrogen atom, as shown in Figs. 6(c) and 6(d). In the first case, layer1(A)-layer2(B), the hydrogen atom desorbs from one sublattice of the first layer, which lies above the center of a hexagon in the second layer, and attaches itself to the closest carbon in the second layer, the potential barrier is only reduced to about 0.91 eV [Fig. 6(c)]. However, for the second case, layer1(B)-layer2(A), the hydrogen atom desorbs from the sublattice of the first layer, which lies above the atoms in the second layer, and then breaks the C-H bond and chemisorbs its opposite carbon atom (nearest neighbour) in the second layer, the potential barrier is only 0.34 eV [Fig. 6(d)]. The hydrogen dissociation energy depends strongly on the separation between the graphene layers. We take it as a dissociation energy because the hydrogen atom dissociates from one of the two graphene layers. The remarkable reduction of barrier is expected to drastically increase the desorption frequency of the confined hydrogen atom, which ensures the direct imaging of the atomic dynamics in our STM measurements.

The potential barrier for the second case is much lower than that of the first case, indicating that the desorption and chemisorption processes prefer to occur on the sublattice above the C atoms in the adjacent graphene sheet, i.e., prefer to occur on one kind of sublattice of graphene. This is in good agreement with our STM observations shown in Fig. 5 and provides further evidence that the H atom is confined between two graphene sheets.

Although the potential barriers of diffusion and desorption for the confined hydrogen atom are much reduced, the reduced

barriers, however, cannot fully account for all the observed phenomena in our STM measurements. Here, we give a rough estimation to illustrate this. With only considering the thermal-driven processes, the diffusion and desorption rate of the H atom intercalated in bilayer graphene can be estimated using the Arrhenius law  $R = \nu \exp(-\frac{E_a}{k_B T})$ , where  $k_B$  is the Boltzmann constant, the prefactor  $\nu$  is a classical attempt frequency (here we use the value  $\nu = 10^{13.6} \text{ s}^{-1}$  according to Ref. [50]), and  $E_a$  is the potential barrier. Based on the theoretical potential barrier, with the electric-field correction taken into account (see the Fig. 7), the calculated desorption rate for the intercalated hydrogen is  $1.17 \times 10^{-6}/\text{s}$ . In our experiment, the average desorption rate for the intercalated hydrogen is estimated to be about  $8 \times 10^{-5}/\text{s}$ . Because there are uncertainties of the prefactor  $\nu$  (it varies for different systems), we should say that the theoretical result is in good agreement with the experimental result. Such a result implies that the thermal-activated processes play a key role in the desorption processes for the intercalated hydrogen. However, this is not the case for the diffusion of the intercalated hydrogen even with taking into account the reduced barriers. The calculated thermally activated diffusion rate is only about  $1 \times 10^{-35}/\text{s}$ , which means that it will take more than millions of years to observe a movement of a hydrogen atom. This differs quite from our experimental result. Our experiment, as shown in Figs. 4 and S4, indicates that the STM tip plays an important role in the diffusion processes. Further experiments will be carried out to quantitatively understand the effects of the STM tip in the dynamics of the intercalated hydrogen atom.

In our experiment, we systematically studied the dynamics of the confined hydrogen atom for more than 30 hours and observed dozens of times its desorption and diffusion between the two graphene sheets. However, the confined hydrogen atom never escapes from the intercalation. Our result provides an atomic-level evidence that graphene is an impermeable atomic membrane at 80 K, even for the lowest-atomic-number H

atom [51–56]. Very recently, Hu *et al.* shows that graphene monolayer is permeable to thermal protons under ambient conditions [57]. They find that the proton-penetration conductivity at 330 K is very high, whereas it almost reduces to zero when the temperature decreases to 270 K. According to their study, the relation of proton-penetration conductivities with the temperature follows Arrhenius-type behavior,  $e^{-E/k_B T}$ . Obviously, thermal fluctuation plays an important role in the penetration. It is also important to emphasize that the barrier of the penetration for physisorption proton is only 1.41 eV (the case in Ref. [57]), however, the potential barrier increases to about 4.54 eV once a C–H bond is formed [58] (our case). Therefore the hydrogen atom cannot penetrate the graphene monolayer in our experiment.

In summary, we directly imaged a hydrogen atom intercalated between two graphene sheets and studied its dynamics systematically. Our STM experiments, complemented by first-principles calculations, indicate that the potential barriers of diffusion and desorption for the confined hydrogen atom are reduced unexpectedly. Such a result suggests that the atomic interfaces of graphene multilayers and other van der Waals materials provide a confined environment to tune the dynamics process of confined atoms or molecules.

This work was supported by the National Natural Science Foundation of China (Grants No. 11674029, No. 11422430, No. 11374035, No. 11334006, and No. 11222436), the National Basic Research Program of China (Grants No. 2014CB920903 and No. 2013CBA01603), the program for New Century Excellent Talents in University of the Ministry of Education of China (Grant No. NCET-13-0054). L.H. also acknowledges support from the National Program for Support of Top-notch Young Professionals and support from “the Fundamental Research Funds for the Central Universities.”

W.-X.W. and Y.-W.W. contributed equally to this work.

- 
- [1] D. C. Elias, R. R. Nair, T. M. G. Mohiuddin, S. V. Morozov, P. Blake, M. P. Halsall, A. C. Ferrari, D. W. Boukhvalov, M. I. Katsnelson, and A. K. Geim, Control of graphene’s properties by reversible hydrogenation: Evidence for graphane, *Science* **323**, 610 (2009).
- [2] R. Balog, B. Jørgensen, L. Nilsson, M. Andersen, E. Rienks, M. Bianchi, M. Fanetti, E. Laegsgaard, A. Baraldi, and S. Lizzit, Bandgap opening in graphene induced by patterned hydrogen adsorption, *Nat. Mater.* **9**, 315 (2010).
- [3] Y. Wang, D. Wong, A. V. Shytov, V. W. Brar, S. Choi, Q. Wu, H. Z. Tsai, W. Regan, A. Zettl, and R. K. Kawakami, Observing atomic collapse resonances in artificial nuclei on graphene, *Science* **340**, 734 (2013).
- [4] O. V. Yazyev, Emergence of magnetism in graphene materials and nanostructures, *Rep. Prog. Phys.* **73**, 56501 (2010).
- [5] J. Balakrishnan, G. K. W. Koon, M. Jaiswal, A. H. C. Neto, and B. Özyilmaz, Colossal enhancement of spin-orbit coupling in weakly hydrogenated graphene, *Nat. Phys.* **9**, 284 (2013).
- [6] H. González-Herrero, J. M. Gómez-Rodríguez, P. Mallet, M. Moaied, J. J. Palacios, C. Salgado, M. M. Ugeda, J. Y. Veuillen, F. Yndurain, and I. Brihuega, Atomic-scale control of graphene magnetism by using hydrogen atoms, *Science* **352**, 438 (2016).
- [7] X. Hong, K. Zou, B. Wang, S. H. Cheng, and J. Zhu, Evidence for Spin-Flip Scattering and Local Moments in Dilute Fluorinated Graphene, *Phys. Rev. Lett.* **108**, 226602 (2012).
- [8] G. Algara-Siller, O. Lehtinen, F. C. Wang, R. R. Nair, U. Kaiser, H. A. Wu, A. K. Geim, and I. V. Grigorieva, Square ice in graphene nanocapillaries, *Nature (London)* **519**, 443 (2015).
- [9] K. S. Vasu, E. Prestat, J. Abraham, J. Dix, R. J. Kashtiban, J. Beheshtian, J. Sloan, P. Carbone, M. Neekamal, and S. J. Haigh, Van der Waals pressure and its effect on trapped interlayer molecules, *Nat. Commun.* **7**, 12168 (2016).
- [10] F. Lei, W. Liu, Y. Sun, J. Xu, K. Liu, L. Liang, T. Yao, B. Pan, S. Wei, and Y. Xie, Metallic tin quantum sheets confined in graphene toward high-efficiency carbon dioxide electroreduction, *Nat. Commun.* **7**, 12697 (2016).
- [11] G. Kresse and J. Hafner, Ab initio molecular dynamics for liquid metals, *Phys. Rev. B* **47**, 558 (1993).

- [12] G. Kresse and J. Furthmüller, Efficient iterative schemes for ab initio total-energy calculations using a plane-wave basis set, *Phys. Rev. B* **54**, 11169 (1996).
- [13] P. E. Blöchl, Projector augmented-wave method, *Phys. Rev. B* **50**, 17953 (1994).
- [14] G. Kresse and D. Joubert, From ultrasoft pseudopotentials to the projector augmented-wave method, *Phys. Rev. B* **59**, 1758 (1999).
- [15] J. P. Perdew, K. Burke, and M. Ernzerhof, Generalized Gradient Approximation Made Simple, *Phys. Rev. Lett.* **77**, 3865 (1996).
- [16] H. J. Monkhorst and J. D. Pack, Special points for Brillouin-zone integrations, *Phys. Rev. B* **13**, 5188 (1976).
- [17] J. Harl, L. Schimka, and G. Kresse, Assessing the quality of the random phase approximation for lattice constants and atomization energies of solids, *Phys. Rev. B* **81**, 115126 (2010).
- [18] G. Henkelman, B. P. Uberuaga, and H. Jónsson, A climbing image nudged elastic band method for finding saddle points and minimum energy paths, *J. Chem. Phys.* **113**, 9901 (2000).
- [19] G. Henkelman, Improved tangent estimate in the nudged elastic band method for finding minimum energy paths and saddle points, *J. Chem. Phys.* **113**, 9978 (2000).
- [20] T. Cai, Z. Jia, B. Yan, D. Yu, and X. Wu, Hydrogen assisted growth of high quality epitaxial graphene on the C-face of 4H-SiC, *App. Phys. Lett.* **106**, 013106 (2015).
- [21] See Supplemental Material at <http://link.aps.org/supplemental/10.1103/PhysRevB.97.085407> for methods, more STM images, STS spectra, and details of the calculations.
- [22] A. C. Ferrari, J. C. Meyer, V. Scardaci, C. Casiraghi, M. Lazzeri, F. Mauri, S. Piscanec, D. Jiang, K. S. Novoselov, and S. Roth, Raman Spectrum of Graphene and Graphene Layers, *Phys. Rev. Lett.* **97**, 187401 (2006).
- [23] A. C. Ferrari and D. M. Basko, Raman spectroscopy as a versatile tool for studying the properties of graphene, *Nat. Nanotechnol.* **8**, 235 (2013).
- [24] C. Riedl, C. Coletti, T. Iwasaki, A. A. Zakharov, and U. Starke, Quasi-Free-Standing Epitaxial Graphene on SiC Obtained by Hydrogen Intercalation, *Phys. Rev. Lett.* **103**, 246804 (2009).
- [25] F. Speck, J. Jobst, F. Fromm, M. Ostler, D. Waldmann, M. Hundhausen, H. B. Weber, and T. Seyller, The quasi-free-standing nature of graphene on H-saturated SiC(0001), *App. Phys. Lett.* **99**, 122106 (2011).
- [26] S. Watcharinyanon, C. Virojanadara, J. R. Osiecki, A. A. Zakharov, R. Yakimova, R. I. G. Uhrberg, and L. I. Johansson, Hydrogen intercalation of graphene grown on 6H-SiC(0001), *Surf. Sci.* **605**, 1662 (2011).
- [27] G. M. Rutter, J. N. Crain, N. P. Guisinger, T. Li, P. N. First, and J. A. Stroscio, Scattering and interference in epitaxial graphene, *Science* **317**, 219 (2007).
- [28] H. Yan, C.-C. Liu, K.-K. Bai, X. Wang, M. Liu, W. Yan, L. Meng, Y. Zhang, Z. Liu, R.-f. Dou, J.-C. Nie, Y. Yao, and L. He, Electronic structures of graphene layers on a metal foil: The effect of atomic-scale defects, *App. Phys. Lett.* **103**, 143120 (2013).
- [29] Y. Zhang, S. Y. Li, H. Huang, W. T. Li, J. B. Qiao, W. X. Wang, L. J. Yin, K. K. Bai, W. Duan, and L. He, Scanning Tunneling Microscopy of the pi Magnetism of a Single Carbon Vacancy in Graphene, *Phys. Rev. Lett.* **117**, 166801 (2016).
- [30] L. Zhao, R. He, K. T. Rim, T. Schiros, K. S. Kim, H. Zhou, C. Gutierrez, S. P. Chockalingam, C. J. Arguello, L. Palova, D. Nordlund, M. S. Hybertsen, D. R. Reichman, T. F. Heinz, P. Kim, A. Pinczuk, G. W. Flynn, and A. N. Pasupathy, Visualizing individual nitrogen dopants in monolayer graphene, *Science* **333**, 999 (2011).
- [31] K.-K. Bai, Y. Zhou, H. Zheng, L. Meng, H. Peng, Z. Liu, J.-C. Nie, and L. He, Creating One-Dimensional Nanoscale Periodic Ripples in a Continuous Mosaic Graphene Monolayer, *Phys. Rev. Lett.* **113**, 086102 (2014).
- [32] M. Z. Hossain, J. E. Johns, K. H. Bevan, H. J. Karmel, Y. T. Liang, S. Yoshimoto, K. Mukai, T. Koitaya, J. Yoshinobu, M. Kawai, A. M. Lear, L. L. Kesmodel, S. L. Tait, and M. C. Hersam, Chemically homogeneous and thermally reversible oxidation of epitaxial graphene, *Nat. Chem.* **4**, 305 (2012).
- [33] G. Li, H. Zhou, L. Pan, Y. Zhang, L. Huang, W. Xu, S. Du, M. Ouyang, A. C. Ferrari, and H. J. Gao, Role of Cooperative Interactions in the Intercalation of Heteroatoms between Graphene and a Metal Substrate, *J. Am. Chem. Soc.* **137**, 7099 (2015).
- [34] J. Wang, D. C. Sorescu, S. Jeon, A. Belianinov, S. V. Kalinin, A. P. Baddorf, and P. Maksymovych, Atomic intercalation to measure adhesion of graphene on graphite, *Nat. Commun.* **7**, 13263 (2016).
- [35] M. Petrović, Š. R. I. S. Runte, C. Busse, J. T. Sadowski, P. Lazić, I. Pletikosić, Z. H. Pan, M. Milun, and P. Pervan, The mechanism of caesium intercalation of graphene, *Nat. Commun.* **4**, 2772 (2013).
- [36] P. Sutter, J. T. Sadowski, and E. A. Sutter, Chemistry under cover: tuning metal-graphene interaction by reactive intercalation, *J. Am. Chem. Soc.* **132**, 8175 (2010).
- [37] L. Jin, Q. Fu, R. Mu, D. Tan, and X. Bao, Pb intercalation underneath a graphene layer on Ru(0001) and its effect on graphene oxidation, *Phys. Chem. Chem. Phys.* **13**, 16655 (2011).
- [38] A. A. El-Barbary, R. H. Telling, C. P. Ewels, M. I. Heggie, and P. R. Briddon, Structure and energetics of the vacancy in graphite, *Phys. Rev. B* **68**, 144107 (2003).
- [39] P. O. Lehtinen, A. S. Foster, Y. Ma, A. V. Krasheninnikov, and R. M. Nieminen, Irradiation-Induced Magnetism in Graphite: A Density Functional Study, *Phys. Rev. Lett.* **93**, 187202 (2004).
- [40] N. P. R. Guisinger, G. M. Crain, J. N. First, P. N. Stroscio, Joseph A, Exposure of epitaxial graphene on SiC (0001) to atomic hydrogen, *Nano Lett.* **9**, 1462 (2009).
- [41] V. P. Tozzini, Prospects for hydrogen storage in graphene, *Phys. Chem. Chem. Phys.* **15**, 80 (2013).
- [42] C. Lin, Yexin Feng, Yingdong Xiao, Michael Dürr, Xiangqian Huang, Xiaozhi Xu, Ruguang Zhao, Enge Wang, Xin-Zheng Li, and Z. Hu, Direct observation of ordered configurations of hydrogen adatoms on graphene, *Nano Lett.* **15**, 903 (2015).
- [43] Y. Ferro, F. Marinelli, A. Jelea, and A. Allouche, Adsorption, diffusion, and recombination of hydrogen on pure and boron-doped graphite surfaces, *J. Chem. Phys.* **120**, 11882 (2004).
- [44] V. A. Borodin, T. T. Vehviläinen, M. G. Ganchenkova, and R. M. Nieminen, Hydrogen transport on graphene: Competition of mobility and desorption, *Phys. Rev. B* **84**, 075486 (2011).
- [45] D. H. Chung, H. Guk, D. Kim, S. S. Han, N. Park, K. Choi, and S.-H. Choi, The effect of the stacking fault on the diffusion of chemisorbed hydrogen atoms inside few-layered graphene, *RSC. Adv.* **4**, 9223 (2014).
- [46] Y. Zhao, J. Wyrick, F. D. Natterer, J. F. Rodriguez-Nieva, C. Lewandowski, K. Watanabe, T. Taniguchi, L. S. Levitov, N. B. Zhitenev, and J. A. Stroscio, Creating and probing electron whispering-gallery modes in graphene, *Science* **348**, 672 (2015).

- [47] Y. Wang, V. Brar, A. Shytov, Q. Wu, W. Regan, H. Tsai, A. Zettl, L. Levitov, and M. Crommie, Mapping dirac quasiparticles near a single coulomb impurity on graphene, *Nat. Phys.* **8**, 653 (2012).
- [48] L. J. Yin, H. Jiang, J. B. Qiao, and L. He, Direct imaging of topological edge states at a bilayer graphene domain wall, *Nat. Commun.* **7**, 11760 (2016).
- [49] J. Petucci, C. LeBlond, M. Karimi, and G. Vidali, Diffusion, adsorption, and desorption of molecular hydrogen on graphene and in graphite, *J. Chem. Phys.* **139**, 044706 (2013).
- [50] L. J. Lauhon and W. Ho, Single molecule thermal rotation and diffusion: Acetylene on Cu(001), *J. Chem. Phys.* **111**, 5633 (1999).
- [51] M. Miao, M. B. Nardelli, Q. Wang, and Y. Liu, First principles study of the permeability of graphene to hydrogen atoms, *Phys. Chem. Chem. Phys.* **15**, 16132 (2013).
- [52] O. Leenaerts, B. Partoens, and F. M. Peeters, Graphene: A perfect nanoballoon, *App. Phys. Lett.* **93**, 193107 (2008).
- [53] V. Berry, Impermeability of graphene and its applications, *Carbon* **62**, 1 (2013).
- [54] L. Tsetseris and S. T. Pantelides, Graphene: An impermeable or selectively permeable membrane for atomic species? *Carbon* **67**, 58 (2014).
- [55] J. S. Bunch, S. S. Verbridge, J. S. Alden, A. M. V. D. Zande, J. M. Parpia, H. G. Craighead, and P. L. McEuen, Impermeable atomic membranes from graphene sheets, *Nano Lett.* **8**, 2458 (2008).
- [56] E. Stolyarova, D. Stolyarov, K. Bolotin, S. Ryu, L. Liu, K. T. Rim, M. Klima, M. Hybertsen, I. Pogorelsky, and I. Pavlishin, Observation of graphene bubbles and effective mass transport, *Nano Lett.* **9**, 332 (2009).
- [57] S. Hu, M. Lozada Hidalgo, F. C. Wang, A. Mishchenko, F. Schedin, R. R. Nair, E. W. Hill, D. W. Boukhvalov, M. I. Katsnelson, and R. A. W. Dryfe, Proton transport through one-atom-thick crystals, *Nature (London)* **516**, 227 (2014).
- [58] V. V. Ivanovskaya *et al.*, Hydrogen adsorption on graphene: A first principles study, *Eur. Phys. J. B* **76**, 481 (2010).